β-delayed γ ray spectroscopy of ^{204,203}Au and $^{202-200}$Pt

A.I. Morales,^{1,*} J. Benlliure,^{1} M. Górska,^{2} H. Grawe,^{2} S. Verma,^{1,†} P.H. Regan,^{3} Zs. Podolyák,^{3} S. Pietri,^{3,‡} R. Kumar,^{4} E. Casarejos,^{1,§} A. Algora,^{5,6} N. Alkhomashi,^{3,¶} H. Álvarez-Pol,^{1} G. Benzoni,^{7} A. Blazhev,^{8} P. Boutachkov,^{2} A.M. Bruce,^{9} L.S. Cáceres,^{2} I.J. Cullen,^{3} A.M. Denis Bacelar,^{9} P. Doornenbal,^{2} M.E. Estévez-Aguado,^{1} G. Farrelly,^{3} Y. Fujita,^{10} A.B. Garnsworthy,^{3} W. Gelletly,^{3} J. Gerl,^{2} J. Grebosz,^{2,**} R. Hoischen,^{11} I. Kojouharov,^{2} N. Kurz,^{2} S. Lalkovski,^{9} Z. Liu,^{12} C. Mihai,^{13} F. Molina,^{5,††} D. Mücher,^{8,‡‡} W. Prokopowicz,^{2,**} B. Rubio,^{5} H. Schaffner,^{2} S.J. Steer,^{3} A. Tamii,^{14} S. Tashenov,^{2} J.J. Valiente-Dobón,^{15} P.M. Walker,^{3} H.J. Wollersheim,^{2} and P.J. Woods^{12}

^{1}*Universidade de Santiago de Compostela, E-15782 Santiago de Compostela, Spain*
^{2}*GSI, Planckstrasse 1, D-64291 Darmstadt, Germany*
^{3}*Department of Physics, University of Surrey, Guildford, GU2 7XH, UK*
^{4}*Inter-University Accelerator Center, New Delhi 110067, India*
^{5}*IFIC, CSIC-Universidad de Valencia, E-46071 Valencia, Spain*
^{6}*Institute of Nuclear Research of the Hungarian Academy of Sciences, Debrecen, H-4001, Hungary*
^{7}*INFN-Sezione di Milano, I-20133 Milano, Italy*
^{8}*IKP, University of Cologne, D-50937 Cologne, Germany*
^{9}*School of Computing, Engineering and Mathematics,*
University of Brighton, Brighton, BN2 4GJ, UK
^{10}*Department of Physics, Osaka University, Toyonaka, Osaka 560-0043, Japan*
^{11}*Department of Physics, Lund University, S-22100 Lund, Sweden*
^{12}*School of Physics and Astronomy, University of Edimburg, Edimburg EH9 3JZ, UK*
^{13}*Horia Hulubei National Institute of Physics and Nuclear Engineering (IFIN-HH), RO-077125 Bucharest-Magurele, Romania*
^{14}*Research Center for Nuclear Physics (RCNP), Osaka University, Japan*
^{15}*INFN-Laboratori Nazionali di Legnaro, I-35020 Legnaro, Italy*
(Dated: February 28, 2013)

The β decay of five heavy, neutron-rich nuclei, ^{204,203}Pt and $^{202-200}$Ir, has been investigated following relativistic cold fragmentation reactions of lead projectiles using the FRS+RISING set up at GSI. This paper reports on the study of the low-lying states in the decay daughter nuclei ^{204,203}Au and $^{202-200}$Pt. The characteristic γ rays for each nucleus have been determined using β-delayed γ ray spectroscopy. Tentative level schemes, relative intensities and apparent β-feedings are provided. These data are compared with shell model calculations, which indicate a substantial contribution to the total β-strength from high energy first-forbidden β-decay transitions in this mass region.

I. INTRODUCTION

The existence of very fast, first-forbidden (FF) β-decay transitions in spherical-like nuclei with low Q_β values close to the doubly magic ^{208}Pb has been established for more than forty years [1]. High energy FF transitions are also expected to appear at increasing neutron number and Q_β. They will play a key role in determining the characteristics of the β decay of r-process nuclei approaching the A∼195 waiting-point [2]. In this region, the first-forbidden ($\nu 3p_{1/2},\pi 3d_{3/2}$), ($\nu 1i_{13/2},\pi 1h_{11/2}$) single-particle configurations dominate over the allowed Gamow-Teller (GT) ($\nu 1h_{9/2},\pi 1h_{11/2}$) decays, mostly blocked because of the low transition energy and the partial filling of the $1h_{11/2}$ proton orbital.

The interpretation of the low-lying excited states of these nuclei in terms of the shell model (SM) [3] can become very complex, since there is a lot of configuration mixing involving valence neutron holes in the $82-126$ shell and valence proton holes in the $50-82$ shell. Such prohibitively large valence spaces have led to the development of several versions of approximations using truncated model spaces [4–8], among which it is worth highlighting the *Interacting Boson Model* (IBM) [5] and the SDG-pair approach of H. Jiang et al. [8].

At variance from the IBM model, which includes correlated and collective pairs of nucleons with spin zero (S) and two (D), the SDG-pair approach also includes nucleon pairs with spin four (G). The model is based

————
*Electronic address: `anaisabel.morales@mi.infn.it`; INFN-Sezione di Milano, I-20133 Milano, Italy
†Department of Physics and Astrophysics, University of Delhi, Delhi 110007, India
‡Present address: GSI, Planckstrasse 1, D-64291 Darmstadt, Germany
§Universidade de Vigo, 36310 Vigo, Spain
¶KACST, P.O. Box 6086, Riyadh 11442, Saudi Arabia
**The Henryk Niewodniczànski Institute of Nuclear Physics, PL-31-342, Kraków, Poland
††Comisión Chilena de Energía Nuclear, P.O.Box 188-D, Santiago, Chile
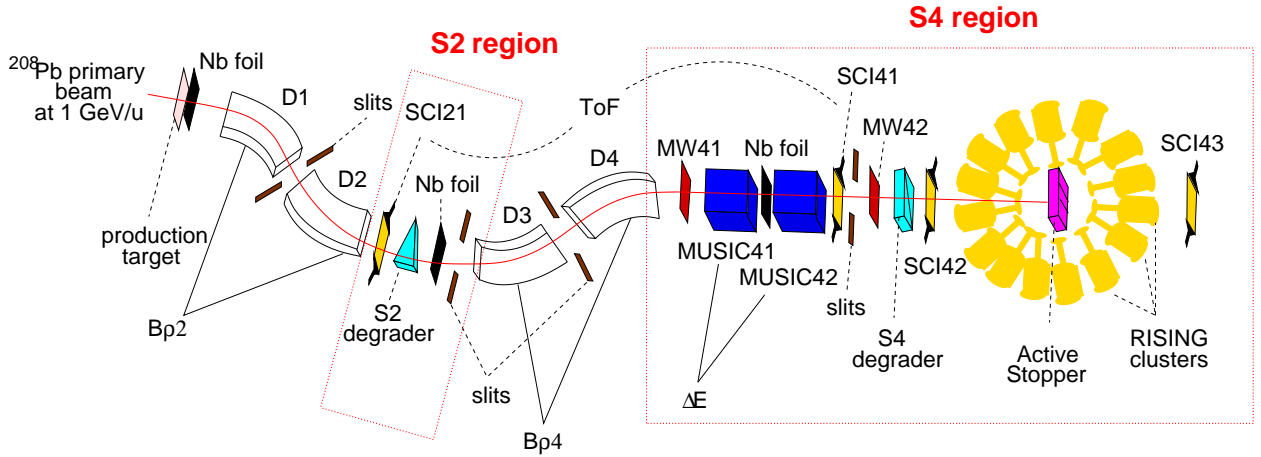‡‡Physik-Department E12, TU München, D-85748 Garching, Germany

FIG. 1: *Schematic of the GSI FRagment Separator and the STOPPED RISING+Active Stopper detection system used for the production, separation, identification and β-delayed γ ray spectroscopy of heavy neutron-rich nuclei [37].*

on a phenomenological shell model Hamiltonian which includes the single-particle energy term, the monopole and quadrupole pairing interactions, and the quadrupole-quadrupole interaction between both like-nucleons and valence protons and neutrons. The Hamiltonian is diagonalized in a collective pair subspace, which is obtained approximating the full shell model space for the low-lying states of the nuclei.

The SDG-pair model has been used recently to calculate the structure at low energy of the Ir, Pt, Au, Hg and Tl isotopes with neutron number N=120-125, and has been shown to provide a quite satisfactory description of their low-lying states, using simple configurations built on the correlated nucleon basis. Consequently, these results are very useful to guide the experimental studies presented in this letter.

The focus of the current work is to investigate the low-lying structure of ^{204,203}Au and $^{202-200}$Pt using β-delayed γ ray spectroscopy. These nuclei are at the current limits of experimental synthesis. Information on nuclei close to ^{208}Pb, though sparse and incomplete, is of importance to determine the onset of collective vibrational motion in heavy systems, as well as to probe the competing theoretical models used in r-process nucleosynthesis calculations [9, 10]. The use of projectile fragmentation at relativistic energies [11] has enabled the investigation of this mass region using the FRS+RISING

setup [12] at GSI, Germany. Preceding this work, experimental studies of these nuclei were centered on the measurement of β-decay half lives [13–19], high-spin decay modes [20–22], and the low-lying excited states of ^{203}Au [23, 24] and ^{200}Pt [25, 26].

The work described here makes use of the FRS+RISING set up in its stopped beam configuration, which incorporates newly developed, state-of-the-art detectors and novel experimental techniques. See for example Refs. [20–22, 27–32] for isomeric studies, and [33–35] for β-delayed γ ray spectroscopy.

II. THE EXPERIMENT

The nuclei investigated in this experiment were produced in cold fragmentation reactions with a ^{208}Pb beam at a primary energy of 1 A GeV, colliding with a Be target of thickness 2.5 g/cm^2. The beam was delivered by the SIS-18 synchrotron [36] at GSI with intensities of up to 10^9 ions/spill and spill lengths of 2 s followed by pauses of 8 s. The fragmentation residues were selected and identified with the double-stage spectrometer FRagment Separator (FRS) [37], appropriately tuned to transmit ^{202}Ir along its central trajectory. A schematic layout of the FRS setup is shown in Fig. 1.

The nuclei of interest were identified according to their mass-over-charge ratio A/Q and their atomic charge state Q. The transverse x-positions of the fragmentation residues at the central (S2) and final (S4) focal planes of the FRS were measured with two plastic scintillators, labeled as SCI21 and SCI41 in Fig. 1. These two detectors provided the stop and the start signals for the time-of-

flight measurement of the ions in the second part of the spectrometer, thus providing an indirect measurement of the mass-over-charge ratio, obtained on an event-by-event basis from the magnetic rigidity $B\rho$ and the velocity v of the nuclei. The atomic charge Q was further derived from the energy loss of every fragment in two MUlti-Sampling Ionization Chambers (MUSIC) located
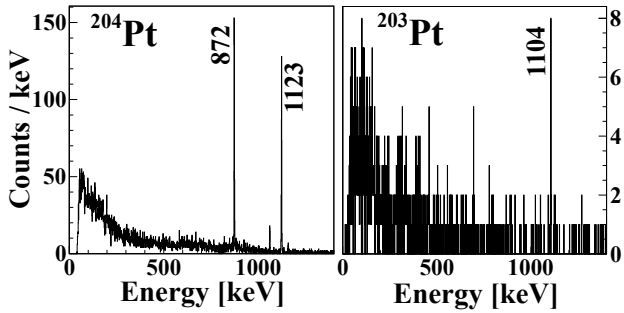
FIG. 2: *Delayed γ ray spectra for ^{204}Pt (left) and ^{203}Pt (right), showing the isomeric transitions reported in [21, 41].*

at the S4 region.

Because the nuclei studied have heavy masses, the changes in charge state undergone by the fragmentation residues in the different layers of matter in the beam line had to be carefully evaluated. The different charge state configurations could be disentangled due to the high energies reached by the SIS-18 synchrotron and the two-stage structure of the FRS. The Al degrader located in the central plane of the separator (see Fig. 1) induced a difference in magnetic rigidity $B\rho$ between the first and second stages that was proportional to the energy loss of the residues in the degrader, ΔE_{deg}. By correlating this variable with the maximum energy loss measured in each of the two MUSIC chambers, Q^{max}, it was possible to determine the different charge state configurations of the nuclei traversing the FRS. Further details on this technique can be found in Refs. [38, 39].

After passing through the spectrometer, the fragments entered into the β-delayed spectroscopy setup, where a variable-thickness Al degrader slowed them down to an energy of several tens of A MeV, enabling their implantation in the RISING active stopper [40]. This process was controlled using the two plastic scintillators located in front of and behind the active stopper, labeled as SCI42 and SCI43 in Fig. 1. The first of these allowed the rejection of nuclei stopped before the active stopper and the resulting secondary reaction products, whereas the second served as a veto scintillator for ions that passed through the stopper.

The RISING active stopper consisted of up to six DSSSD detectors of dimensions $5 \times 5 \times 0.1$ cm^3, each with 16 strips on both the front and back sides, giving 256 pixels that provided the energy, time and position of fragments and β-like particles. In the current experiment, the active stopper included only three DSSSD pads, two of them set up one behind the other in the central position and the other set to the right side of the central trajectory. This device was used to correlate implantations with β-decay electrons in position and time. In previous works it was also employed to identify the delayed conversion electron lines following internal decay [42].

Due to the wide dynamic range needed to detect heavy fragments with energies over 1 GeV and electron signals of less than 1 MeV, semi-logarithmic preamplifiers [43] were used in the electronic chain, with a linear response for low-energy signals (1-10 MeV) and a logarithmic amplification for high-energy events (10 MeV- 3 GeV) [40].

The RISING γ ray array, in its *Stopped Beam Configuration* [44], surrounded the active stopper. This array, consisting of fifteen cluster detectors with seven germanium crystals each, had a photopeak efficiency of 15% at 662 keV [44]. It registered the energy and time of the γ rays emitted by the implanted nuclei and their daughters, enabling time correlations of up to 400 μs between both implantations and γ rays and β-like particles and γ rays. In order to reduce the Compton background of the β-delayed γ ray energy spectra, the energy signals registered in the crystals of a given Ge-cluster were summed if they were within a time interval of 200 ns.

Though the focus of this work is the identification of the electromagnetic transitions following the β decay of the fragmentation residues, the isomeric decays in ^{204,203}Pt were studied with the aim of confirming the identification procedure. Figure 2 illustrates the isomeric γ ray energy spectra of these nuclei, where the isomeric transitions previously reported in [21, 41] can be observed.

The use of a monoenergetic degrader at the central focal plane of the FRS provided a horizontally-dispersed beam with a confined range distribution in the beam direction [45]. This feature improved the efficiency of the active stopper and increased the probability of implanting several nuclear species per pixel. The high segmentation of the DSSSD pads was thought to address this challenge. Nevertheless, the long half lives of the nuclei under study, of the order of tens of seconds [46], constrained the analysis to correlation times longer than the beam cycle. This limitation, together with the high implantation rates, gave rise to multiple implantation events within the ion-β correlation time, inducing activity build-up of random ion-β correlations coming from daughters or nuclei with overlapping implantation distributions. Figure 3 shows the transverse x-position distributions of the fragmentation residues in the active stopper. $M1$, $M2$ refer to the middle front and middle rear DSSSD pads, respectively, whereas R refers to the silicon detector on the right hand side. As can be seen, at least two nuclear species impinged on the same range of X-strips in the three DSSSD detectors.

III. ANALYSIS PROCEDURE

The analysis of the β-delayed γ ray spectra was based on a event-by-event identification of the implanted nuclei in atomic and mass number (Z,A), their individual pixel position in the active stopper (X,Y), the β-like particle pixel position (x,y), and the time of detection of implantations, β-decays and characteristic γ rays.
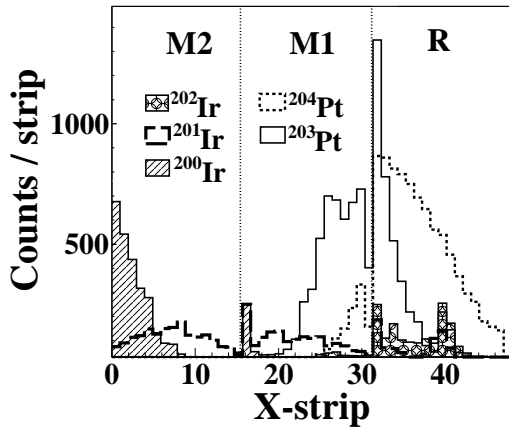
FIG. 3: *Transverse x-position distributions of the fragmentation residues implanted in the active stopper.*

Valid implantation events were defined using three conditions. The first was a high energy signal in the SCI42 front-scintillator, the second no energy signal in the SCI43 veto scintillator, and the third a logarithmic high-energy signal in an individual pixel (X,Y) of the active stopper. Since the range of the β-like electrons in this device was greater than the pixel size, valid β-like events were defined by a signal above 150 keV in the pixel of implantation or one of the eight neighbor cells, within a time interval equivalent to three half-life periods. Lifetime measurements for the fragmentation residues of interest are reported in a parallel publication [46]. Electromagnetic transitions were accepted within a maximum correlation time of 200 ns after the detection of the matching β-like electron.

False correlations between implantations and β-like particles appeared because of the δ-electrons generated during the slowing down process of the fast charged ions in the DSSSD pads. These events were suppressed by selecting only the β-like particles registered during the 8 s beam pause. Since the measured half lives are longer than the length of the beam pulse, making the time correlations only during the beam pauses was not an important constraint.

In order to separate the characteristic γ rays of the selected nucleus from the "cocktail" of random peaks coming from neighboring or daughter nuclei, only the first valid β-like electron detected in the pixel activated by the implantation was accepted. Though such restrictive conditions reduced significantly the statistics of the data analysis, the identification of the most intense γ-ray tran-

sitions of each nuclear specie was unequivocal.

The background was evaluated with a new energy spectrum, sorting the reversed time sequence of ion-β correlations (henceforth referred to as *backward-time* or *time-reversed* energy spectrum). As the backward-time correlations are accidental, they represent the background of the energy spectra in normal time direction (henceforth referred to as *forward-time* spectra) under the same experimental conditions. Note that this procedure is purely qualitative, since the background is normalized to the number of forward-time ion-β correlations, no matter if they are real or false.

The time-reversed energy spectra of ^{203}Pt and ^{201}Ir, two nuclei with implantation rates of the order of the β-decay time, had a strong contribution from *"true" backward-time correlations.* These events are defined as correlations in the inverse-time sequence that connect randomly a given fragment with a true β-electron, thus introducing true γ-decays in the background spectra. Also due to the high implantation rates of these nuclei, the forward-time energy spectra were strongly contaminated by random correlations with β-decays from neighboring fragments. In these cases, the qualitative evaluation of the characteristic (or background) γ-peaks was carried out in the region of the active stopper with the higher number of mother (or background) nuclei, according to the position distributions shown in Fig. 3. The particular sorting conditions for each nucleus will be discussed in the next section.

The spectroscopic study also involved the analysis of $\gamma\gamma$ coincidences. In this case, all the valid β-like particles were accepted, independently of their time or position. The only condition required was a time correlation interval between coincident γ rays of up to 100 ns.

IV. RESULTS

Using the technique described in the previous section, we were able to investigate the low-lying excited states of ^{204,203}Au and $^{202-200}$Pt populated in the β-decay of their respective progenitors.

Figure 4 shows the β-delayed γ ray energy spectra of the five nuclei under discussion. The γ rays characterizing each of them are indicated in bold, whereas x-rays or other residual transitions are shown in italics. With the exception of ^{201}Pt, the qualitative background (see above) has been subtracted from the singles energy spectra. A total of 41 γ ray transitions are reported, of which 34 have been observed for the first time.

The background-subtracted spectrum of the four-hole nucleus $^{204}_{79}$Au$_{125}$, shown in the upper panel of Fig. 4, has been obtained from the forward- and backward-time ion-

β correlations detected in the right DSSSD pad. The forward correlations have been restricted to the right part of the detector, where mainly ^{204}Pt is implanted (see
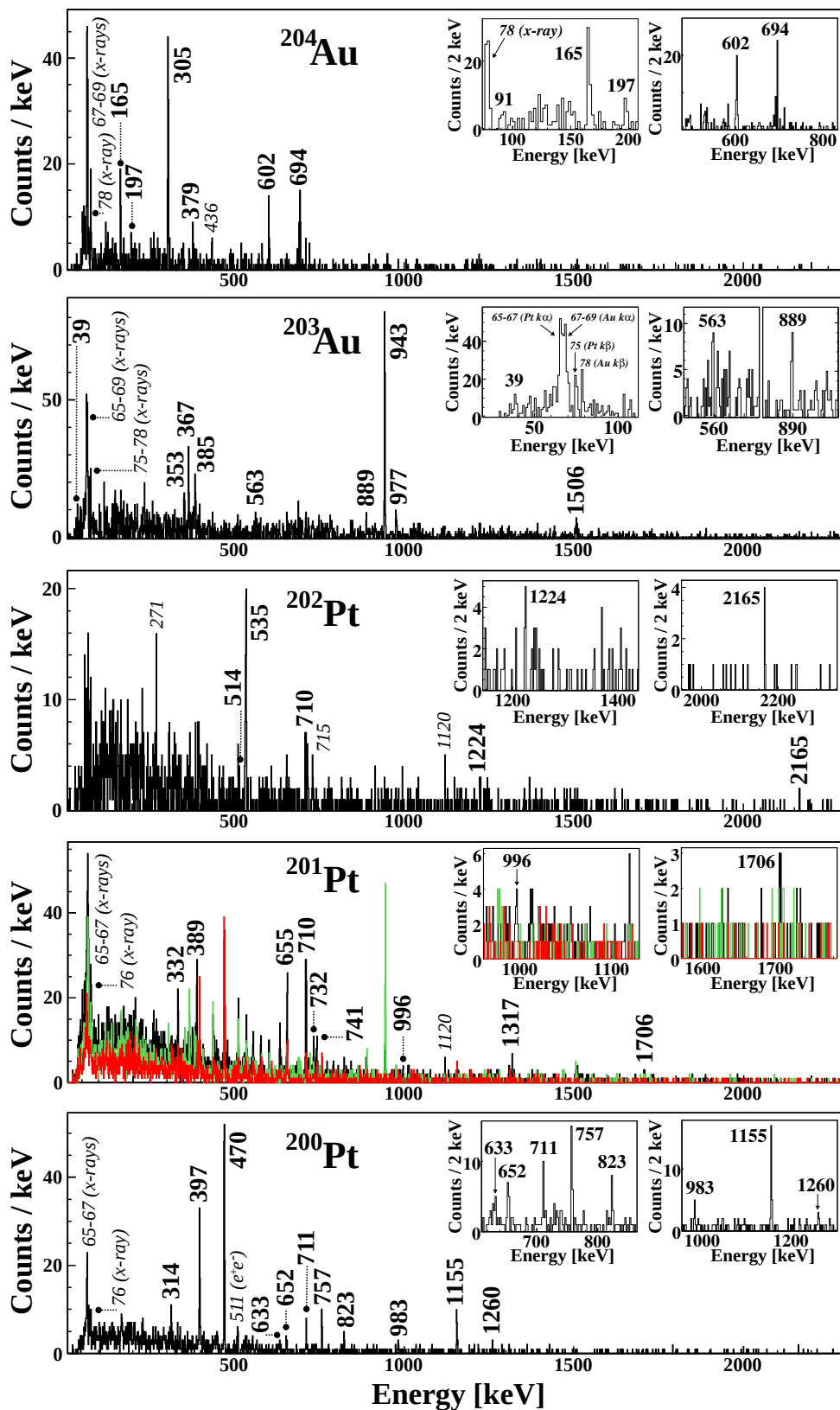
FIG. 4: *(Color online) From top to bottom, γ ray energy spectra of* ^{204}Au, ^{203}Au, ^{202}Pt, ^{201}Pt *and* ^{200}Pt, *populated after the β-decay of their precursors. The γ rays characterizing each nucleus are indicated in bold, whereas x-rays or other residual transitions are shown in italics. The particular sorting conditions for each spectrum are discussed in the text.*

Fig. 3). The corresponding backward-time correlations, aimed to reproduce the contribution from ^{203}Pt and ^{202}Ir in this region of the active stopper, have been performed in the same pixel as the forward sequence, since the implantation rates of ^{204}Pt, 0.024 s^{-1}, are smaller than its β-decay constant, 0.043 s^{-1}, and thus the contribution of "true" backward-time correlations is negligible. As a result, six new γ-ray peaks have been observed associated with this decay.

In ^{203}Pt, the similarity between the implantation rates of the nucleus (0.038 s^{-1}) and its β-decay constant (0.032 s^{-1}) blocks correlations in the pixels of implantation of the residues, since a part of the random, time-uncorrelated β-like electrons come from the decay of their precursors. In order to overcome this limitation, when a nucleus of ^{203}Pt is implanted in the front-central DSSSD detector, the time-reversed correlation is performed with a β-like particle of the rear-middle DSSSD. Since in the right DSSSD only the tail of the distribution impinges on the pad, the implantation rates drop off significantly and the correlation can be done in the pixel of implantation of the ion. The resulting background-subtracted spectrum is shown in the second upper panel of Fig. 4. For this nucleus, nine out of ten γ ray transitions are reported for the first time. The only γ-peak reported in the literature is the 563 keV transition, observed in the isomeric studies of Caamaño et al. [20].

In ^{202}Ir, the rates of implantation, 0.0055 s^{-1}, are about a factor ten smaller than the β-decay constant, 0.046 s^{-1}. Consequently the contribution of random coincidences is negligible and the background-subtracted spectrum can be obtained with the usual forward (backward) time sequences, i.e., with the correlations between each implantation and the next (previous) valid β-electron registered in the same cell. The background-subtracted spectrum of ^{202}Pt is shown in the third panel of Fig. 4. Excepting the $2_1^+ \rightarrow 0_{g.s.}^+$ γ ray at 535 keV [20], all the transitions observed provide new structural information on this N=124 isotone.

The γ ray energy spectrum of ^{201}Pt is shown in the fourth panel of Fig. 4. In this case, the rates of implantation and β-decay are equal (0.033 s^{-1}), and most of the random backward-time β-like electrons come from its own β decay. The forward-time spectrum, represented in black, is restricted to the implantations detected in the front middle DSSSD pad. The backward-time correlations are built from the implantation profiles of the contaminant residues (see Fig. 3): if the implantation is registered in the right half of the pad, the time-reversed correlation is performed in the pixel where the forward-time correlation was detected. This spectrum, shown in green in Fig. 4, includes the random contributions from ^{204,203}Pt and ^{202}Ir. The main contaminant on the left side of the detector is ^{200}Ir. In order to reproduce the γ-ray transitions from its daughter (^{200}Pt), the ^{201}Pt residues are correlated with a β-like electron of the rear middle DSSSD. This last spectrum is shown in red in the figure. Though the backward-time contribution is purely

qualitative, the nine peaks that emerge from the background have been assigned tentatively to ^{201}Pt.

Looking at Fig. 3, one can observe that only ^{201,200}Ir reach the rear central DSSSD pad. The energy spectrum shown at the bottom of Fig. 4 was sorted with the forward-time correlations restricted to the left part of the detector, since most of the ^{200}Ir nuclei were deposited there, with a negligible amount of ^{201}Ir. As a result, eleven γ-peaks have been identified as characteristic transitions of ^{200}Pt, five of which (470, 397, 314, 633 and 711 keV) are reported in the literature [26]. The other transitions have been detected for the first time following the β decay of ^{200}Ir.
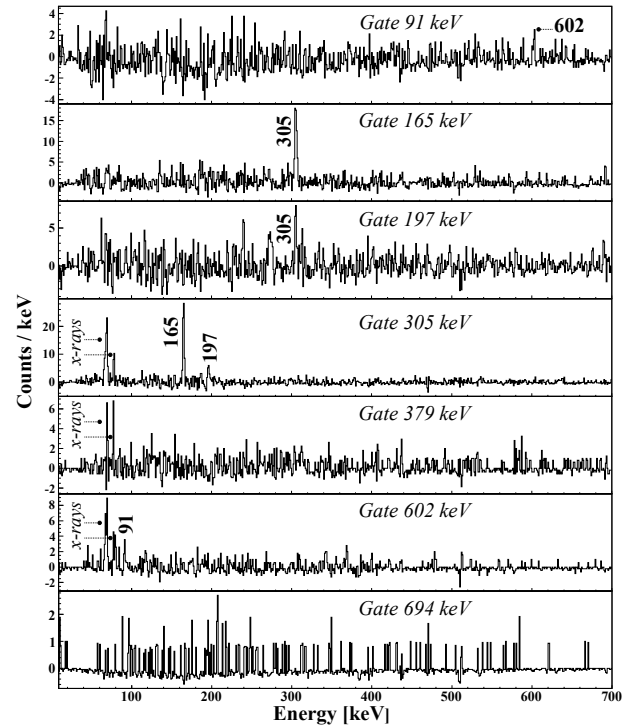

FIG. 5: *From top to bottom: β-delayed $\gamma\gamma$ coincidence spectra gated on the 91, 165, 197, 305, 379, 602 and 694 keV transitions of ^{204}Au. Note that the 91 keV γ-peak is seen above background in coincidence with the 602 keV transition, but not in the singles energy spectrum of Fig. 4.*

The $\gamma\gamma$ coincidence analysis provides further spectroscopic information on the nuclei under study. As an illustration, Fig. 5 displays the $\gamma\gamma$ coincidence spectra gated on the 91, 165, 197, 305, 379, 602 and 694 keV transitions of ^{204}Au. In these spectra, the transition at 602 keV, observed in the β-delayed singles spectrum of ^{204}Au (see Fig. 4), shows mutual coincidence with a low intensity 91 keV γ ray, not seen above the background in Fig. 4. Based on this, the new 91 keV transition has also been considered to be in the partial decay scheme of ^{204}Au.

Similarly, the $\gamma\gamma$ coincidence spectra of ^{203}Au and ^{202}Pt reveal further low-intensity γ rays; the 311 and 776 keV transitions in the case of ^{203}Au, and the 718 and 1048

keV γ-peaks for ^{202}Pt. For the former nucleus, the 311 keV transition plays an important role in its shell model interpretation, as discussed in the next section. In the case of ^{202}Pt, the 718 keV γ-peak, under the background in the singles spectrum of Fig. 4, is reported as the $4_1^+ \rightarrow 2_1^+$ transition in [20]. Its observation in coincidence with the 535 keV transition gives us confidence in the $\gamma\gamma$ coincidence analysis, and accounts for the inclusion of these γ rays in the tentative decay patterns.

The tentative low-lying level schemes have been built from the β-delayed and $\gamma\gamma$ coincidence spectra. Figures 6 and 7 show the partial decay schemes of ^{204,203}Au and $^{202-200}$Pt, respectively. The level scheme of ^{202}Pt has been built from the mutual coincidence of the $2_1^+ \rightarrow 0_{g.s.}^+$ 535 keV γ ray [20] with all the other transitions, while that of ^{200}Pt arises from coincidences with the $2_1^+ \rightarrow 0_{g.s.}^+$ 470 keV γ-peak [20] and the other observed γ rays.

Relative transition intensities (I_t^{rel}) and apparent β-feedings (I_β) have been deduced. The corresponding values are provided in table I. For each tentative level the apparent β-feeding is calculated indirectly, as the ratio between the γ-feeding of the state and the total γ-ray transition intensity observed, thus giving an idea of how many times a level is populated directly by β decay. In turn, the γ-feeding of each state is defined as the difference between the total γ-ray transition intensity de-exciting the level and the γ-ray intensity that feeds the level. It is worth noting that the absolute efficiency of the germanium detectors has been taken into account in all these measurements. The detection efficiency of the β-particles is unknown in the current work and, consequently, the I_β values given in table I do not include the direct population of the ground states. This is a good approximation for ^{204}Au and ^{202,200}Pt, since the high momentum transfers ($J \geq 2$) hinder the β-feeding to the ground states [1]. For ^{203}Au and ^{201}Pt, the values provided can be used for guidance, though they should be revised following further experiments.

V. DISCUSSION

In this section, the results are discussed in a shell model framework using the code OXBASH [47], and are further compared to the SDG-pair approach [8].

For the Au isotopes, the shell model calculations were performed assuming a ^{208}Pb inactive core plus a model space consisting of the $1h_{9/2}$, $2f_{7/2}$, $2f_{5/2}$, $3p_{3/2}$, $3p_{1/2}$ and $1i_{13/2}$ hole configurations for neutrons and the $1g_{7/2}$, $2d_{5/2}$, $2d_{3/2}$, $3s_{1/2}$ and $1h_{11/2}$ hole orbitals for protons. The single-particle energies and effective residual interaction used were taken from [48]. These parameters were previously used as standard input in the shell model calculations of ^{206}Hg, ^{205}Au and ^{204}Pt, reproducing adequately the observed excited states [21, 42, 49]. Other nuclei in the region, including both proton and neutron configurations were also satisfactorily explained using the same interaction [22].

In the case of the Pt isotopes, the SM calculations posed a computational challenge due to the very large valence spaces involved. For the 2-neutron, 4-proton hole nucleus ^{202}Pt, two nucleon bases were used; the former, labeled as SM in Figs. 6 and 7, comprised all the single-particle orbitals in the $Z = 50 - 82$, $N = 82 - 126$ shells; the latter, labeled as SM2, excluded the orbitals $\nu 1h_{9/2}$ and $\pi 1g_{7/2}$ lying deepest in the shell, and the high-spin $\nu 1i_{13/2}$ orbital, which are expected to play a minor role in the structure of the low-spin states populated in β decay. For ^{201}Pt, with 3 neutron- and 4 proton-holes out of the ^{208}Pb core, only the truncated valence space could be used, while for ^{200}Pt, with 8 nucleon-holes, the truncated SM calculations became prohibitive, and, consequently, the observed structure has been interpreted merely in terms of the SDG-pair estimates.

Because of the large number of holes involved, the level densities in these nuclei are very high. They induce strong configuration mixing in the calculated states that block any firm, definite assignment of the spin-parity J^π of the experimental levels. However, the states here observed were populated following β decay, and the β interaction in the region nearby the doubly-magic ^{208}Pb is characterized by very fast, high-transition energy FF decays [1], mostly due to the opening of the $(\nu 3p_{1/2}, \pi 3d_{3/2})$, $(\nu 1i_{13/2}, \pi 1h_{11/2})$ configurations [2]. For these nuclei the forbidden transitions of higher order are negligible and the β interaction can be expressed in moments of multipole order 0 or 1. Furthermore, the contribution of unique transitions with angular momentum transfer $\Delta J = 2$ is expected to be lower than 1% and can be also neglected [2]. As a consequence, the β-decay selection rules limit the range of possible J^π values.

In the following, we perform a detailed discussion on the tentative J^π assignments for each nucleus.

A. β-decay ^{204}Pt $\rightarrow$ ^{204}Au

The low-lying level scheme of ^{204}Au is shown in Fig. 6, together with the SM calculations using the full valence space.

The potential existence of β transitions from the isomeric levels in ^{204}Pt is excluded on the basis that the only isomers reported [21, 22] are about six to eight or-

Nucleus	J^π	E_s (keV)	E_γ (keV)	$I_t^{rel}(\%)$	$I_\beta(\%)$
^{204}Au	(1^-)	305.7(1.1)	305.7(1.1)	100(8)	17(6)
	$(1^-, 2^-)$	379.3(1.9)	379.3(1.9)	18(2)	7.2(1.9)
	(1^-)	471(2)	165(2)	46(4)	19(5)
	$(1^-, 2^-)$	503(2)	197.0(1.7)	11.7(1.3)	4.7(1.2)
	$(1^-, 2^-)$	602.4(1.9)	602.4(1.9)	65(6)	7(9)
	$(0^-, 1^-)$	694(2)	91.6(1.0)[1]	47(18)	45(11)
			694.7(0.9)	63(6)	
^{203}Au	$1/2^+$	39.0(0.9)	39.0(0.9)[2]	117(17)	10(13)
	$3/2^+$	385(2)	385(2)	17.4(1.4)	4.0(1.7)
	$(7/2^+)$	563(2)	563(2)	8.5(0.9)	1.5(0.6)
	$(3/2^+)$	874(5)	311(5)	6.0(0.6)	3.7(0.8)
	$(1/2^+)$	976.8(1.6)	976.8(1.6)	6.1(0.8)	3.7(0.9)
	$(1/2^+)$	982.6(1.5)	943.6(1.2)	100(7)	61(13)
	$(1/2^+, 3/2^+, 5/2^+)$	1161(4)	776(4)	4.1(0.6)	2.5(0.6)
	$(1/2^+, 3/2^+, 5/2^+)$	1275(3)	889.0(1.5)	6.7(0.9)	4.1(1.0)
	$(1/2^+, 3/2^+)$	1505.8(1.3)	1505.8(1.3)	15.7(1.7)	10(2)
^{202}Pt	(2^+)	535.0(1.3)	535.0(1.3)	100(8)	8(18)
	(2^+)	1245(2)	710.1(1.5)	52(5)	24(35)
	(4^+)	1253.7(1.9)	718.7(1.4)	3.8(1.0)	4(2)
	(1^+)	1583.0(1.8)	1048.0(1.2)	10.0(1.9)	10(6)
	$(1^+, 3^+)$	1759(4)	514(3)	28(3)	43(26)
			1224.0(1.9)	15(2)	
	$(2^-, 3^-)$	2700.0(1.7)	2165.0(1.1)	11(2)	11(7)
^{201}Pt	$(1/2^-, 3/2^-, 5/2^-)$	332.6(1.7)	332.6(1.7)	31(3)	13.1(1.9)
	$(1/2^-, 3/2^-, 5/2^-)$	389.4(1.5)	389.4(1.5)	26(3)	6.2(1.9)
	$(1/2^-, 3/2^-, 5/2^-)$	655(2)	655(2)	100(8)	42(6)
	$(1/2^-, 3/2^-, 5/2^-)$	710.1(1.5)	710.1(1.5)	46(4)	5(3)
	$(1/2^-, 3/2^-, 5/2^-)$	741(2)	741(2)	22(3)	9.2(1.5)
	$(1/2^-, 3/2^-, 5/2^-)$	1442(3)	732(2)	28(3)	12.0(1.9)
	$(1/2^-, 3/2^-, 5/2^-)$	1706(2)	996.5(1.6)	5.0(1.2)	12.0(1.6)
			1317(2)	11(2)	
			1706(2)	12(2)	
^{200}Pt	(2^+)	470.1(1.2)	470.1(1.2)	100(7)	24(14)
	$(2)^+$	867(2)	397.3(1.6)	42(3)	0(8)
	4^+	1103(2)	632.5(1.9)	13.0(1.5)	13(4)
	$(3)^+$	1181(2)	313.7(1.4)	7.5(0.9)	8(2)
			711	2.5(0.6)	
		1625(3)	757(2)	12.4(1.6)	29(6)
			1155.0(1.6)	16(2)	
	$(2)^+$	1690(3)	822.9(1.7)	8.6(1.3)	9(3)
	(2^+)	1730.4(1.4)	1260.3(0.7)	2.3(0.7)	2.3(1.0)
		1833(3)	652.3(1.1)	2.2(0.6)	2.2(0.9)
	(2^+)	1850(3)	982.9(1.5)	13.3(1.8)	13(4)

TABLE I: Proposed spin-parities, level energies, γ ray energies, relative transition intensities and β-decay feeding of each state related to the nuclei investigated in this work. [1]: $\alpha_{tot}(M1)=9.5(4)$. [2]: $\alpha_{tot}(M1)=20.5(3)$.

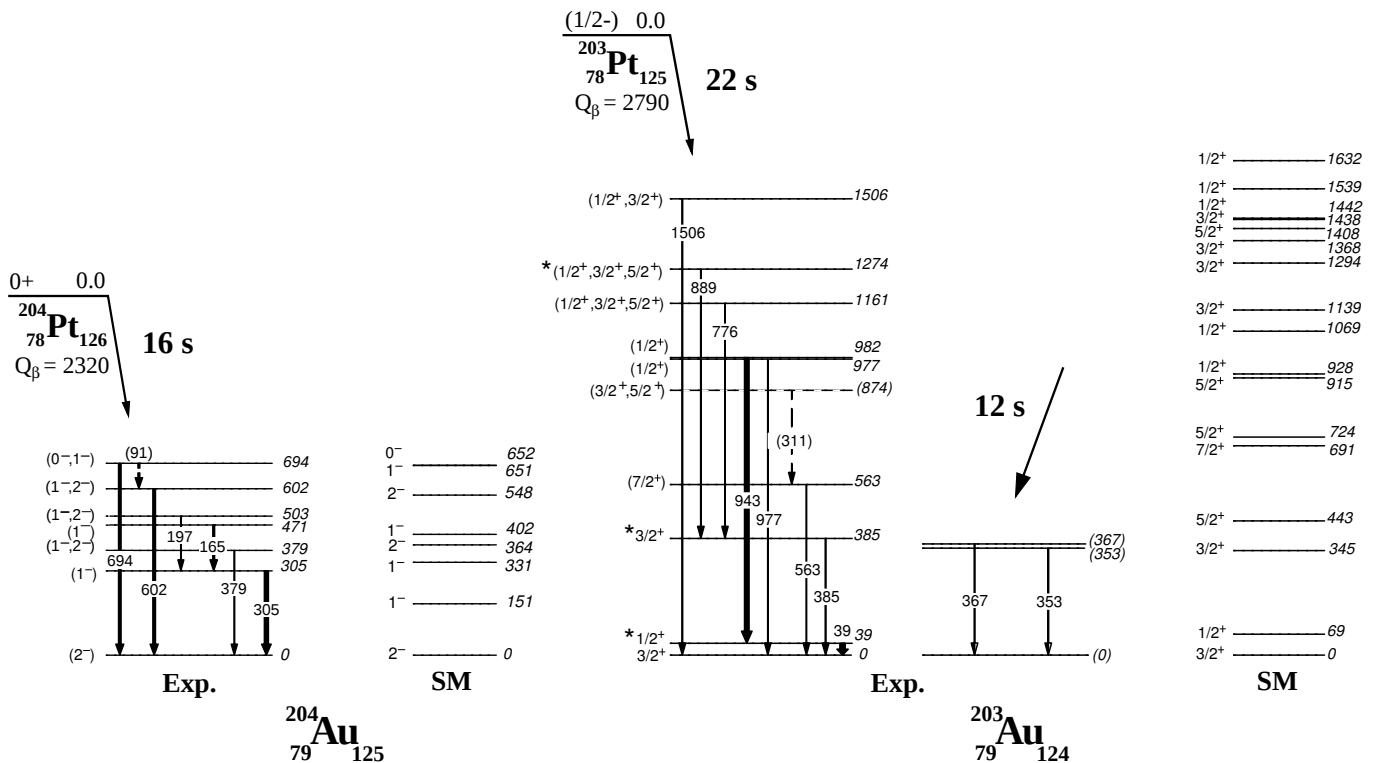FIG. 6: *Experimental and calculated partial level schemes of the Z = 79 isotopes ^{204}Au and ^{203}Au. Arrow widths denote relative intensities, normalized to the most intense transition. The states marked with an asterisk were reported in Refs. [23, 24]. SM represents calculations using the shell model code OXBASH. Half lives and Q_β values taken from [46] and [50], respectively.*

ders of magnitude faster than the β decay time, 16 s [46]. Furthermore, the theoretical SM calculations for this work do not predict the existence of any isomeric transition with a lifetime of tens of seconds. In addition, β transitions from the 0^+ ground state (g.s.) of ^{204}Pt to long-lived nuclear levels in ^{204}Au are ruled out because of the large angular momentum transfers needed.

The theoretical SM approach predicts the existence of no positive-parity states with angular momentum transfer $\Delta J=0$ or 1 within the Q_β energy window, suggesting that all the β transitions have a forbidden character. Assuming a dominant role for the FF decays, the transitions with highest intensity are expected to decay to $J^\pi=(0^-)$ or (1^-) states in ^{204}Au. Excited states with $J^\pi=(2^-)$, instead, are expected to appear with rather small transition rates. From the apparent β-feedings reported in table I, the states at 379, 503 and 602 keV are proposed as good (2^-) candidates, provided that part of their feeding comes from the de-excitation of higher-lying, unobserved levels in ^{204}Au that are also populated in β decay. In any case, a hypothetical spin-parity (1^-) is not excluded. Note that the SM calculations predict two $J^\pi=2^-$ states in the experimental energy range. This is still consistent with the apparent β-feedings of table I, since the I_β value of the 602 keV state was measured assuming an M1 character for the 91 keV γ ray. Any variation in the character of this transition will increase

the intensity of the β-branch to the 602 keV state, thus the other two levels, 379 and 503 keV, are suggested to be the matching experimental partners of the two theoretical 2^- states. The strong β-feeding to the rest of the states suggests tentative $J^\pi=(0^-)$ or (1^-) assignments.

The SDG-pair approach [8] also predicts two 2^- levels within the experimental energy range, though placed much closer together than in the SM. Typically, the states are lowered in energy, with differences ranging from 150-200 keV in the case of the 1^- levels up to 600 keV for the 0^- states.

Though the energy of the first excited state is notably reduced in both calculations, the character of the nuclear levels can be generally understood in terms of their wave functions, which underline the spherical-like structure of this A=204 isotone.

B. β-decay ^{203}Pt $\rightarrow$ ^{203}Au

The experimental level scheme of ^{203}Au is shown in Fig. 6, together with the structure calculated from the SM approach. The states labeled with an asterisk were previously reported in the literature with an energy resolution of 30 keV [24].

The most striking feature of this nucleus is the appearance of two γ-ray transitions at 353 and 367 keV with an

associated β decay of 12(5) s. Instead, the half-life of the nuclear levels firmly assigned to ^{203}Au is 22(4)s [46]. This dilemma can be resolved provided that the mother ^{203}Pt has a long-lived, metastable state of several seconds decaying to the corresponding levels. The SM calculations of this work predict the existence of two isomers. The first is a long-lived $J^\pi=13/2^+$, 1484 keV state of the order of several hundred ms that might decay through an E3 transition to the $7/2_1^-$ at 1210 keV. According to the selection rules of the β interaction, the $13/2^+$ isomer can only feed the $11/2^-$ metastable state in ^{203}Au, reported in the literature at 641 keV [23, 24]. Experimental isomeric spectroscopy of this nucleus [22] reveals a 563 keV γ ray with a half life of 140(44) μs, interpreted as connecting the reported $11/2^-$ 641 keV isomer to the $(7/2^+)_1$ 563 keV state through an unobserved M2 transition. In our β-decay studies, however, the 563 keV γ ray is not observed at times longer than the sensitivity of the DGF electronics, 200 ns [44]. This upper limit for the lifetime of the state excludes its population through the $11/2^-$ isomer. As a result, there is no experimental evidence for the population of the $13/2^+$ state in ^{203}Pt.

The second isomer of ^{203}Pt predicted by the SM is a $27/2^-$ yrast trap calculated to lie at an energy of 2954 keV. Shell model calculations suggest that it can decay by a low-energy E4 transition to a $19/2^-$ state at 2626 keV or by an 820 keV M4 decay to a $19/2^+$, 2134 keV state. An E5 transition to a $17/2^+$ level at 2244 keV is also possible, though the predicted lifetime is much longer than the one observed in the present work. The calculated conversion coefficients for the E4 and M4 transitions are respectively $\alpha_T = 1.66$ and $\alpha_T = 0.24$, which indicate that the isomeric trap can deexcite either internally, through highly converted transitions registered as β-like electrons, or following β decay. In the first case the 353 or 367 keV γ rays could connect the yrast trap with the $13/2^+$ isomer. In the second case, the β decay would proceed more likely through a FF transition to the $25/2^+$ state in ^{203}Au, calculated at 2759 keV. This level would decay through a low-energy M1 transition to the $23/2^+$ state at 2731 keV. The sequential decay to the g.s. or to the $11/2^-$ isomer in ^{203}Au is not observed in this case, as it might happen if the β-decay branch is weak. Internal decay of the $25/2^+$ level to the ground state cannot be either justified by the SM theory, since the OXBASH calculations only predict one state beneath 400 keV, the $3/2_2^+$ 345 keV state. As previous studies locate it between 386-389 keV [23, 24], the 385 keV γ ray observed

in the singles energy spectrum has been proposed as its de-excitation to the g.s., leaving no clear interpretation of the structures associated with the 353 and 367 keV γ rays. Anyhow, the model space employed in the SM calculations does not account for the existence of a core excited isomer across the 126-neutron shell, which could very likely justify the appearance of the 353 and 367 keV γ-ray transitions.

For this nucleus, the assignment of spin-parities has been made according to the reported spectroscopic information [23, 24] and the β-decay selection rules described before. The values of spin given in brackets in Fig. 6 are consistent with the SM calculations, but cannot be firmly determined. In the case of the 563 keV level, we have kept the $(7/2^+)$ spin assignment given in [22], provided that it arises from a FF transition connecting the $(1/2^-)$ g.s. of ^{203}Pt to a higher-lying $(3/2^+)$ or $(5/2^+)$ state in ^{203}Au. This interpretation is justified because of the mutual coincidence of the 563 keV transition with the 311 keV γ ray, not observed in the singles energy spectrum of Fig. 4. The corresponding nuclear level is located at 874 keV. The γ-feedings of these two states, shown in table I, are consistent with the β-decay transition selection rules within two standard deviations.

It is worth noting that the SM approach predicts an inversion of the $11/2^-$ and $7/2_1^+$ states in ^{203}Au, with the first being at 622 keV and the second at 691 keV. In this case, the $\pi h_{11/2}^{-1}$ isomer would decay through an E4 transition of approximately 3 s for a Weisskopf unit to the ground state. Therefore the interpretation provided by Ref. [22] seems more likely to be in line with both the isomeric studies and the observations of the present work.

Comparison with SDG-pair predictions leads, more or less, to the same conclusions. In this case, the $13/2^+$ isomer of ^{203}Pt and the $11/2^-$ isomer of ^{203}Au are expected to lie 300 and 500 keV higher than in the SM calculations. For ^{203}Pt, two $9/2^-$ states are located below the long-lived $J^\pi=13/2^+$ isomer, suggesting a lifetime of the order of ns, whereas for ^{203}Au the location of the $11/2^-$ and $7/2_1^+$ states suggests a lifetime of tens of nanoseconds, compatible with the half life observed in this work for the 563 keV transition, but not with that measured in the isomeric studies of [22]. Anyhow, the location of the states up to 700 keV is approximately the same for both models, suggesting, despite the complex interpretation of some nuclear states, an underlying spherical structure.

C. β-decay ^{202}Ir $\rightarrow$ ^{202}Pt

The experimental level scheme of ^{202}Pt is shown in Fig. 7. The proposed nuclear levels have been deduced from the $\gamma\gamma$ coincidence analysis, since all the transitions are in mutual coincidence with the reported $2_1^+ \rightarrow 0_{g.s.}^+$ 535

keV γ ray [20]. Two shell model calculations are also shown in the figure as SM and SM2 (see introduction to Sec. V). The theoretical schemes include the negative-parity states with angular momentum transfer $\Delta J=0$ or 1 lying within the experimental energy range, since low-energy GT transitions might arise due the large Q_β of
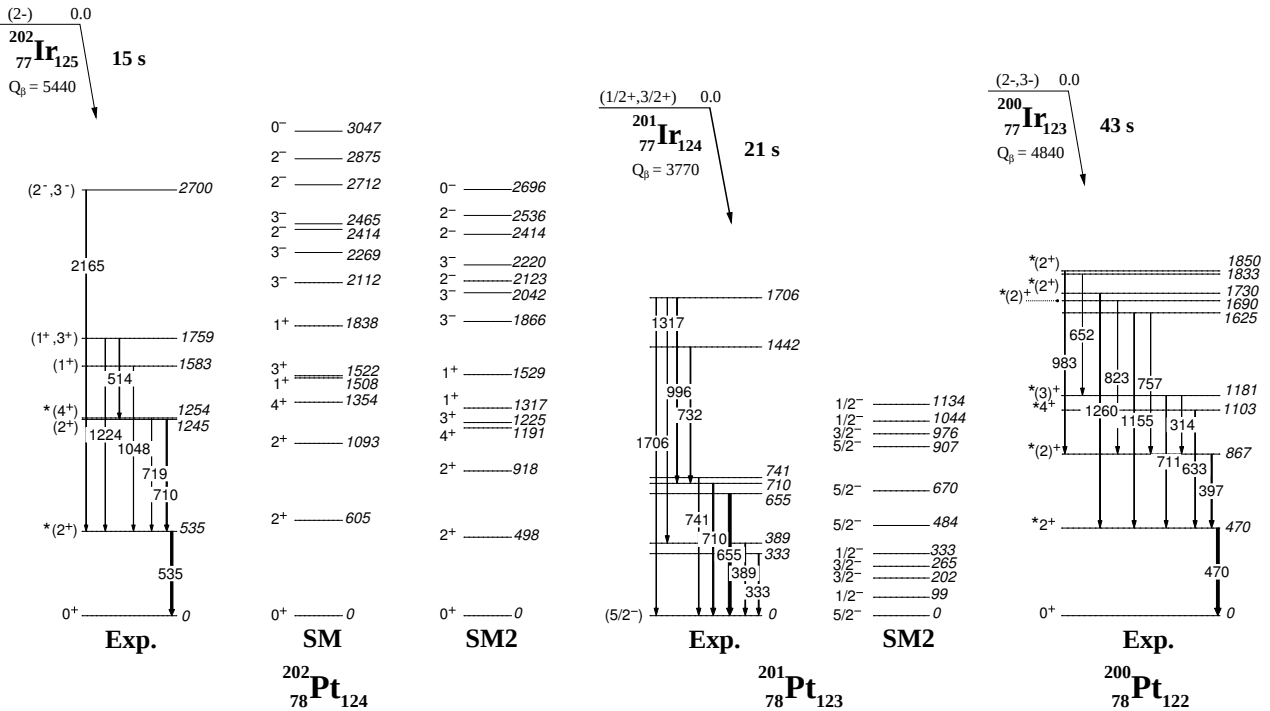
FIG. 7: *Experimental and calculated partial level schemes for the Z = 78 isotopes ^{202}Pt, ^{201}Pt and ^{200}Pt. Arrow widths denote relative intensities, normalized to the most intense transition. The states marked with an asterisk were reported in Refs. [20, 25, 26]. SM represents calculations using the shell model code OXBASH, whereas SM2 are with the truncated model space, as described in the text. Half lives and Q_β values taken from [46] and [50], respectively.*

the mother ^{202}Ir.

At first sight, one can observe that the truncated decay diagram is compressed in energy. This effect is to be expected, since the residual interaction strength between pairs of nucleons (or holes) in identical orbitals, namely the pairing strength, is smaller for medium and low j-orbitals.

In general, the margin of error of the states calculated with the full model space is less than 160 keV; this is not the case for the first excited 2^- and 3^- levels, calculated to lie respectively about 300 keV and 600 keV below the experimental candidate. Due to these large deviations, the assignment of spin-parities in Fig. 7 is only tentative. Note that a $J^\pi=(1^+,3^+)$ assignment has been proposed for the 1759 keV level as it lies between the 1^+ and 3^+ calculated states.

The spin-parity of the g.s. in the mother ^{202}Ir is expected to be (1^-) or (2^-) from the systematics of neighboring nuclei. Though the small β-feeding of the $(4^+)_1$ state -shown in table I- suggests a $J^\pi=(2^-)$, the (1^-) assignment cannot be definitely excluded on the basis that the $(4^+)_1$ level might be fed in the de-excitation of unobserved higher-lying states weakly populated in β decay.

The appearance of a high energy nuclear state at 2700 keV with a significant β intensity suggests that it is populated directly through an allowed β transition. This in-

terpretation is supported by the large energy gap to the subsequent nuclear states. Based on these arguments, we propose a tentative $J^\pi=(2^-,3^-)$ for this level.

The location of the nuclear states is significantly lower in the SDG-pair approach than in the SM, with the difference being larger at increasing energies. In particular, the 2_3^+ and 3_1^+ levels drop beneath the 4_1^+. In our β-decay studies, however, only two states are observed below the 4_1^+, both of them with large β-feedings. They seem more likely to be the 2_1^+ and 2_2^+ states, in agreement with the SM calculations. No information is given in [8] about the negative-parity levels.

There are two remarkable characteristics of this nucleus. On the one hand, both high-transition energy FF and low-transition energy GT decays seem to compete in the β decay, as shown by the spin-parities proposed from SM calculations. On the other hand, the 2^+-2^+-0^+ cascade typical of the O(6) limiting symmetry of the IBM model [5] is observed. Such a cascade is not normally expected in even-even spherical-like nuclei because relatively high-lying 2^+ states decay to the ground state rather than decaying only to other 2^+ level. Its observation is suggestive of the onset of collective vibrational excitations. This argument is supported by the de-excitation modes of the $(1^+,3^+)$ level: the γ-ray transition to the second (2^+) state is more intense than the

decay to the first (2^+) level, as table I shows. Such a feature can be explained in terms of the quantum number selection rules of the IBM model [51].

D. β-decay ^{201}Ir $\rightarrow$ ^{201}Pt

The experimental level scheme of ^{201}Pt is shown in Fig. 7, together with the nuclear structure calculated with the truncated SM approach. The strong compression of the calculated states, originating from the suppression of the high-spin orbitals $\nu 1i_{13/2}$, $\nu 1h_{9/2}$ and $\pi 1g_{7/2}$, prevents any spin-parity assignment. Nevertheless, in a SM framework, the observed levels are expected to have $J^\pi = (1/2^-), (3/2^-)$ or $(5/2^-)$. Only the tentative $(5/2^-)$ spin has been kept for the g.s., according to SM and SDG calculations, and the systematics of neighboring N=123 nuclei. Assignments of spins $(1/2^-)$ and $(3/2^-)$ cannot be unambiguously excluded however.

Empirically, the two lowest groups of experimental states in ^{201}Pt (333-389 keV and 655-741 keV in Fig. 7) seem to constitute the multiplets generated by the coupling of the neutron hole of odd-parity to the $(2^+)_1$ and $(2^+)_2$ levels in ^{202}Pt. This assumption is further supported by the wave functions of the SM2 calculation: the main components of the $(5/2^-)_2$, $(5/2^-)_3$ states are, respectively, $\nu 3p_{3/2}$ and $\nu 4s_{1/2}$ configurations coupled to the first (2^+). In the case of the $(5/2^-)_4$ state, the unpaired neutron hole mainly occupies the $\nu 2f_{5/2}$ orbital coupled to the $(2^+)_2$ state of ^{202}Pt. Similarly, the $(1/2^-)_2$ and $(3/2^-)_2$, $(3/2^-)_3$ levels arise from coupling the unpaired neutron hole to the (2_1^+) level in ^{202}Pt, and the $(1/2^-)_3$, $(1/2^-)_4$ and $(3/2^-)_4$ from coupling it to the $(2^+)_2$. In addition, the two highest states observed in ^{201}Pt could arise from the coupling of the extra neutron to the group of (2^+) states identified in ^{200}Pt at similar energies. Nevertheless all the calculated wave functions are highly mixed, with the squares of the amplitude of the leading components having about 10-20%.

In the case of the mother ^{201}Ir, the g.s. spin-parity is expected to be $(1/2^+)$ or $(3/2^+)$ from the systematics of the neighboring isotones, though the SM and the SDG-pair approaches predict $J^\pi_{g.s.}$=$3/2^+$.

In summary, the β decay picture of the previous nuclei seems to be kept, since negative-parity transitions with angular momentum transfers ΔJ=0,1 or, to a lesser extent, ΔJ=2 are expected from SM and SDG estimates.

E. β-decay ^{200}Ir $\rightarrow$ ^{200}Pt

The eight valence holes out of the ^{208}Pb core prevent us performing SM calculations for ^{200}Pt, not even using the truncated model space SM2. Figure 7 shows the experimental level scheme of this nucleus, built from the singles energy spectrum of Fig. 4 and the $\gamma\gamma$ coincidence analysis. Except for the state at 1833 keV, all the nuclear levels populated following β decay are reported in

[25, 26]. The J^π values shown in the figure are taken from these references.

The g.s. of the mother ^{200}Ir is expected to have $J^\pi = (0^-, 1^-, 2^-)$ from the systematics of the neighboring N=122 isotones, although higher spins of negative parity cannot be unambiguously excluded. The absence of the 0^+, 1583 keV level [26] and the strong β-feeding of the 4^+ state set aside the $J^\pi = (0^-, 1^-)$ candidates. In addition, the observed feeding of the $(2)_3^+$, $(2^+)_4$ and $(2^+)_5$ states, shown in table I, and the absence of the $(5)^-$ 1567 keV level [20] suggest that negative-parity spins higher or equal than (4^-) can also be excluded. As a consequence, the g.s. spin-parities proposed from the present work are $(2^-, 3^-)$.

As in ^{202}Pt, the SDG-pair approach predicts the 2_3^+ state below the 4_1^+. In our β-decay studies, however, only the two previously reported 2_1^+ and $(2)_2^+$ levels are observed. Except for this, the agreement with the experimental levels is quite good.

The similarity with ^{202}Pt is further exhibited in some of the transition sequences observed: the 983 and 823 keV γ rays unexpectedly connect two (2^+) states with the $(2)_2^+$ level, whereas the corresponding transitions to the 2_1^+ state are unobserved. Also the 2^+-2^+-0^+ cascade with strong E2 transitions discussed for the ^{202}Pt isotope is seen. As previously mentioned, such features can be explained in terms of the phonon quantum number selection rules of the IBM approach [51].

VI. CONCLUSIONS

Low-lying excited states have been observed in ^{204,203}Au and ^{202,201,200}Pt, using β-delayed γ ray spectroscopy of the fragmentation residues ^{204,203}Pt and ^{202,201,200}Ir, respectively.

The character of the excited states has been investigated in terms of the shell model, revealing the underlying spherical structure of ^{203,204}Au. Further comparison with the SDG-pair approach supports this idea, though generally the nuclear states are lowered in energy in the calculations. In the case of ^{202}Pt, the agreement of the experimental and calculated states still suggests a spherical-like character, though some structural properties typical of pairing vibrational excitations in collective systems have been observed, such as the 2_2^+-2_1^+-0^+ cascade or the unexpectedly favored decay of some states to the non-yrast 2_2^+ level rather than to the 2_1^+ state. Such features, derived in a natural way from the quantum number selection rules of the Interacting Boson Model [51], have also been observed in ^{200}Pt.

Though the decay patterns cannot be firmly established from this work, the SM interpretation of ^{203,204}Au and ^{202}Pt supports strongly the "forbidden" β-decay picture in the region near the doubly-magic ^{208}Pb. In the particular case of ^{204}Au, the SM theory shows that all the GT states lie outside the Q_β window, whereas for ^{202}Pt the large feeding of the 2700 keV state suggests a

low energy GT decay competing with the FF transitions. Also from SM estimates, strong negative-parity decays with angular momentum transfers ΔJ=0,1 are expected to appear in ^{201}Ir. For ^{200}Ir, FF transitions are also expected from the systematics of the g.s. in neighboring N=122 isotones and the large β-feeding of some positive-parity states in ^{200}Pt.

In general, the important role of the FF decays in nuclei with low and medium Q_β approaching the shell N=126 can be discerned from the results of this work. If this tendency is maintained in the r-process nuclei around the A$\sim$195 waiting-point, a theory describing adequately the contribution from high energy FF transitions to the total β-strength will be vital for the understanding of this process of nucleosynthesis.

[1] J. Damgaard et al., Nucl. Phys. A 135, 310 (1969)
[2] I.N. Borzov, Phys. of Atom. Nucl. 8 (2011)
[3] M.G. Mayer, Phys. Rev. 75, 1969 (1949)
[4] I. Talmi, Nucl. Phys. A 172, 1 (1971)
[5] F. Iachello and A. Arima., The Interacting Boson Model, Cambridge University Press (1987)
[6] K. Allaart et al., Phys. Rep. 169, 209 (1988)
[7] Y.M. Zhao et al., Phys. Rev. C 80, 061302 (2009)
[8] H. Jiang, J.J. Shen, Y.M. Zhao and A. Arima, J. Phys. G, Nucl. Part. Phys. 38, 045103 (2011)
[9] P. Möller, B. Pfeiffer and K.-L. Kraft, Phys. Rev. C 67, 055802 (2003)
[10] I.N. Borzov, Phys. Rev. C 67, 025802 (2003)
[11] J. Benlliure et al., Nucl. Phys. A 660, 87 (1999)
[12] P.H. Regan et al., Int. Jour. Mod. Phys. E 17, 8 (2008)
[13] A. Pakkanen, T. Komppa and H. Helppi, Nucl. Phys. A 184, 157 (1972)
[14] D.A. Craig et al., J. Phys. G, Nucl. Phys. 10, 1133 (1984)
[15] Ch. Wenneman et al., Z. Phys. A 347, 185 (1994)
[16] S. Shi, W.D. Huang, Y. Li, D.Z. Yin, J.H. Gu and J.Q. Tian, Z. Phys. A 342, 369 (1992)
[17] J. Facetti, E. Trabal, R. McClin and S. Torres, Phys. Rev. 127, 1690 (1962)
[18] K.P. Gopinathan, M.C. Joshi, and M. Radhamenon, Nuovo Cimento 30, 14 (1963)
[19] John C. Hill, D.G.Shirk, R.F. Petry and K.H.Wang, Phys. Rev. C 13, 2484 (1976)
[20] M. Caamaño et al., Eur. Phys. J. 23, 201 (2005)
[21] S.J. Steer et al., Phys. Rev. C 78, 061302 (2008)
[22] S.J. Steer et al., Phys. Rev. C 84, 044313 (2011)
[23] E.R. Flynn, Ronald E. Brown, J.W. Sunier and J.M. Gursky, Phys. Lett. B 105, 125 (1981)
[24] P. Grabmayr, A. Mondry, G.J. Wagner and P. Woldt, Phys. Rev. C 49, 2971 (1994)
[25] J.A. Cizewski et al., Phys. Rev. C 23, 1453 (1981)
[26] S.W. Yates et al., Phys. Rev. C 37, 1889 (1988)
[27] R. Grzywacz et al., Phys. Rev. C 55, 1126 (1997)
[28] C. Chandler et al., Phys. Rev. C 61, 044309 (2000)
[29] Z. Podolyàk et al., Nucl. Phys. A 722, 273 (2003)
[30] Z. Podolyàk et al., Phys. Lett. B 633, 203 (2006)
[31] N. Al-Dahan et al., Phys. Rev. C 62, 014304 (2009)
[32] A. Gottardo et al., Phys. Rev. Lett. 109, 162502 (2012)
[33] N. Alkhomashi et al., Phys. Rev. C 80, 064308 (2009)
[34] N. Al-Dahan et al., Phys. rev. C 85, 034301 (2012)
[35] G. Benzoni et al., Phys. Lett. B 715, 285 (2012)
[36] M. Steiner et al., Nucl. Instr. and Meth. A 312, 420 (1992)
[37] K.-H. Schmidt et al., Nucl. Instr. and Meth. A 260, 287 (1987)
[38] A.I. Morales et al., Phys. Rev. C 84, 011601 (2011)
[39] E. Casarejos et al., Phys. Rev. C 74, 044612 (2006)
[40] R. Kumar et al., Nucl. Instr. and Meth. A 598, 754 (2009)
[41] S.J. Steer et al., Acta Phys. Pol. B 38, 1283 (2007)
[42] Z. Podolyàk., Phys. Lett. B 672, 116 (2009)
[43] http://www.mesytec.com
[44] S. Pietri et al., Nucl. Instr. and Meth. B 261, 179 (2007)
[45] T. Kurtukián-Nieto et al., Nucl. Instr. and Meth. A 589, 472 (2008)
[46] A.I. Morales et al., in preparation
[47] B.A. Brown, A. Etchegoyen, N. Godwin, W. Rae, W. Richter, W.E. Ormand, E. Warburton, J. Winfield, L. Zhao and C. Zimmerman C, MSU-NSCL Report No.524 (1985) and MSU-NSCL Report No.1289 (2004)
[48] L. Rydström, J. Blomqvist, R.J. Liotta and C. Pomar. Nucl. Phys. A 512, 217 (1990)
[49] B. Fornal et al., Phys. Rev. Lett. 87, 21 (2001)
[50] P. Möller, J.R. Nix and K.-L. Kratz., Atomic Data Nucl. Data Tables 66, 131, (1997)
[51] A. Arima and F. Iachello., Ann. Phys. (N.Y.) 123, 468 (1979)